ELSEVIER

Journal of Fluids and Structures 26 (2010) 1–18

JOURNAL OF FLUIDS AND STRUCTURES

www.elsevier.com/locate/jfs

Effect of velocity ratio on the streamwise vortex structures in the wake of a stack

M.S. Adaramola[a,1], D. Sumner[b,*], D.J. Bergstrom[b]

[a]*Division of Environmental Engineering, University of Saskatchewan, 57 Campus Drive, Saskatoon, Saskatchewan, Canada S7N 5A9*
[b]*Department of Mechanical Engineering, University of Saskatchewan, 57 Campus Drive, Saskatoon, Saskatchewan, Canada S7N 5A9*

Received 16 September 2008; accepted 4 August 2009
Available online 7 October 2009

Abstract

The time-averaged velocity and streamwise vorticity fields within the wake of a stack were investigated in a low-speed wind tunnel using a seven-hole pressure probe. The experiments were conducted at a Reynolds number, based on the stack external diameter, of $Re_D = 2.3 \times 10^4$. The stack, of aspect ratio AR = 9, was mounted normal to a ground plane and was partially immersed in a flat-plate turbulent boundary layer, where the ratio of the boundary layer thickness to the stack height was $\delta/H \approx 0.5$. The jet-to-cross-flow velocity ratio was varied from $R = 0$ to 3, which covered the downwash, crosswind-dominated and jet-dominated flow regimes. In the downwash and crosswind-dominated flow regimes, two pairs of counter-rotating streamwise vortex structures were identified within the stack wake. The tip vortex pair located close to the free end of the stack, and the base vortex pair located close to the ground plane within the flat-plate boundary layer, were similar to those found in the wake of a finite circular cylinder, and were associated with the upwash and downwash flow fields within the stack wake, respectively. In the jet-dominated flow regime, a third pair of streamwise vortex structures was observed, referred to as the jet-wake vortex pair, which occurred within the jet-wake region above the free end of the stack. The jet-wake vortex pair had the same orientation as the base vortex pair and was associated with the jet rise. The peak vorticity and strength of the streamwise vortex structures were functions of the jet-to-cross-flow velocity ratio. For the tip vortex structures, their peak vorticity and strength reduced as the jet-to-cross-flow velocity ratio increased.

Keywords: Bluff-body aerodynamics; Finite circular cylinder; Chimney stack; Elevated jet in cross-flow; Wake; Vortex structures

1. Introduction

The simplest stack geometry can be represented by a uniform-diameter circular cylinder of finite height mounted normal to a ground plane. The separated flow field of a finite circular cylinder is complex and strongly three-dimensional, due to the flow around the base (the cylinder–wall junction) and over the free end (Kawamura et al., 1984; Okamoto, 1991; Tanaka and Murata, 1999; Sumner et al., 2004; Adaramola et al., 2006; Wang et al., 2006). There are

*Corresponding author. Tel.: +1 306 966 5537; fax: +1 306 966 5427.
E-mail addresses: muyiwa.adaramola@ntnu.no (M.S. Adaramola), david.sumner@usask.ca (D. Sumner).
[1]Present address: Department of Energy and Process Engineering, Norwegian University of Science and Technology, Trondheim, Norway.

0889-9746/$ - see front matter © 2009 Elsevier Ltd. All rights reserved.
doi:10.1016/j.jfluidstructs.2009.07.007

marked changes in the near-wake flow structure along the cylinder height and these changes are strongly influenced by the cylinder's aspect ratio, AR ($= H/D$, where H and D are the height and diameter of the cylinder, respectively), and the relative thickness of the flat-plate boundary layer on the ground plane, δ/H or δ/D (where δ is the boundary layer thickness at the location of the cylinder). When the aspect ratio exceeds a critical value (which depends on δ/H and other parameters), two pairs of counter-rotating streamwise vortex structures are found within the wake of the finite circular cylinder (Tanaka and Murata, 1999; Sumner et al., 2004). The first pair, called the tip vortex structures, is formed close to the free end, while the second pair, known as the base vortex structures, is found within the flat-plate boundary layer on the ground plane close to the base of the cylinder. The tip vortex structures interact in a complex manner with Kármán vortex shedding from the sides of the cylinder, and are responsible for a downward-directed local velocity field near the free end referred to as "downwash." The base vortex structures, on the other hand, induce an "upwash" velocity field closer to the ground plane (Sumner et al., 2004; Adaramola et al., 2006; Wang et al., 2006). A localized region of low mean streamwise velocity and high turbulence intensity is found behind the cylinder, centred between the four main streamwise vortex structures (Adaramola et al., 2006). The location of the tip vortex structures has been shown to depend on the ground plane boundary layer thickness (Wang et al., 2006).

Compared with a finite circular cylinder, the presence of a jet flow issuing from the stack (see Fig. 1) gives rise to an even more complicated flow structure, both around the stack and in its wake. The behaviour of a turbulent round jet discharged normally into a cross-flow depends on how the jet is injected and, for a non-buoyant jet flow, the jet-to-cross-flow velocity ratio, R ($= U_e/U_\infty$, where U_e is the average jet exit velocity and U_∞ is the freestream velocity). The jet can be injected through either an orifice on the ground plane, which is referred to as ground-level source jet, or from an elevated source, as in the case of the stack. There is extensive work on the ground-level source jet in the literature (e.g., Moussa et al., 1977; Andreopoulos and Rodi, 1984; Fric and Roshko, 1994; Smith and Mungal, 1998; Lim et al., 2001; Wegner et al., 2004; New et al., 2006). For a ground-level source jet, four distinct vortical structures have been

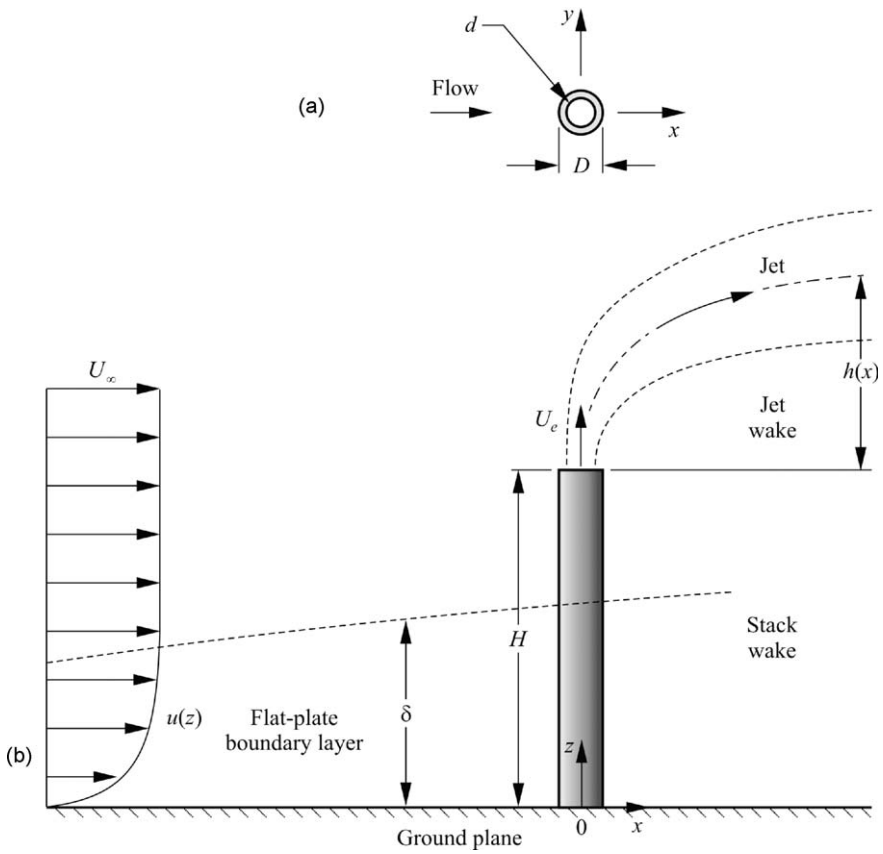

Fig. 1. Stack of uniform circular cross-section (of external diameter, D, internal diameter, d, and height, H) mounted normal to a ground plane and partially immersed in a turbulent flat-plate boundary layer (with thickness, δ, streamwise velocity profile, $u(z)$, and freestream velocity, U_∞): (a) top view; (b) side view.

identified (e.g., Fric and Roshko, 1994; Smith and Mungal, 1998): horseshoe vortices, the jet shear layer or leading-edge vortices (Lim et al., 2001), the wake structures and the counter-rotating vortex pair. In addition to the velocity ratio effect, the inclination of the jet flow also has an effect on the jet behaviour and the impact of the cross-flow on it. For instance, Wegner et al. (2004) reported that for $R = 0.5$, the jet mixing and the strength of the counter-rotating vortex pair increase with the angle of the inclination of the jet to the cross-flow. For the elevated jet in cross-flow, representing a stack, the local flow field is characterized by the complex interactions between the jet and stack wakes, shear produced by the upward momentum of the jet, and downwash flow. Following the definition of Eiff and Keffer (1999) and Adaramola et al. (2007), the stack wake is defined as the region $0 < z/H \leq 1$ (where x is the streamwise coordinate, y is the cross-stream coordinate, and z is the wall-normal coordinate, with the origin at the base of the stack, as shown in Fig. 1), while the jet wake is defined as the region $z/H > 1$.

Much of the attention in the stack literature has focused on the jet rise [e.g., Overcamp and Ku (1988)], since the dispersion of pollutants is the primary purpose of a stack. In contrast, there are relatively few studies that present detailed measurements in the near-wake or the local flow field of the stack. Of the available studies that present velocity measurements (Eiff et al., 1995; Johnston and Wilson, 1997; Eiff and Keffer, 1997, 1999; Huang and Hsieh, 2002, 2003; Mahjoub Saïd et al., 2005, 2007; Adaramola et al., 2007), they have generally been restricted to localized regions of the flow field, such as velocity profiles within the jet-wake region (Eiff et al., 1995; Eiff and Keffer, 1999), or velocity measurements within a vertical plane on the wake centreline (Huang and Hsieh, 2002, 2003; Mahjoub Saïd et al., 2005, 2007).

The flow topology in the vertical plane along the stack wake centreline (the x–z plane, Fig. 1(b)) has been used to classify the stack and jet-wake flow patterns into a number of flow regimes based on the approximate value of R. Huang and Hsieh (2002, 2003), using a stack of $\mathrm{AR} = 25$, identified four flow regimes: (i) downwash flow ($R < 0.95$), (ii) crosswind-dominated flow ($0.95 < R < 1.4$), (iii) transitional flow ($1.4 < R < 2.4$), and (iv) jet-dominated flow ($R > 2.4$). A similar study of the local flow field of a small-aspect-ratio stack of $\mathrm{AR} = 8.3$, by Mahjoub Saïd et al. (2005), identified three zones within the jet: zone 1, immediately above the stack exit, where the jet dominates the flow; zone 2, where the jet begins to bend and the jet flow and cross-flow have the same velocity; and zone 3, further downstream, where the cross-flow dominates the flow. Depending on the value of R and the corresponding flow regime, one or more of these zones may be absent.

Few studies of the stack flow field have considered wake velocity measurements within vertical planes normal to the streamwise direction (the y–z plane), further downstream of the jet exit. Adaramola et al. (2007) studied a small-aspect-ratio stack of $\mathrm{AR} = 9$, which was partially immersed in a flat-plate turbulent boundary layer, and used hot-wire anemometry to measure the turbulent wake for $R = 0$ to 3. Based on their near-field velocity measurements obtained in the y–z plane, the behaviour of the stack was broadly classified into three flow regimes; adopting the terminology used by Huang and Hsieh (2002, 2003), these flow regimes were classified as the downwash ($R < 0.7$), the crosswind-dominated ($0.7 \leq R < 1.5$), and the jet-dominated ($R \geq 1.5$) flow regimes. Each flow regime had a distinct structure to the mean velocity fields and Reynolds stresses (Adaramola et al., 2007). They also reported a strong influence of R on the variation of the Strouhal number, St ($= f_s D/U_\infty$, where f_s is the Kármán vortex shedding frequency), along the stack height. For $R \geq 1.5$, they observed a two-cell structure behaviour in the Strouhal number along the height of the stack. In agreement with Eiff et al. (1995) and Eiff and Keffer (1997, 1999), for a stack of $\mathrm{AR} = 8$, the value of St within the stack and jet wakes was the same (for a given value of R), which suggested that similar vortices (or a single vortex structure) were being shed in both wakes. Moussa et al. (1977) also reported that the vortex shedding from the jet is controlled by the Kármán vortex shedding from the sides of the stack.

The complex nature of the wake structure of this flow and its significant variation with R, combined with the limited velocity measurements presented in the literature, together are motivation for further study of the local flow field of the stack. Information is also lacking on the behaviour of the streamwise vortex structures within the stack wake. These structures are known to have an important role in the problem of stack downwash (Johnston and Wilson, 1997), which occurs at low jet-to-cross-flow velocity ratios, yet they have not been extensively investigated in the literature. Further information on these structures will therefore contribute to an improved physical overall understanding of the stack wake and the downwash phenomenon. As a first step towards this understanding, a seven-hole pressure probe is used in the present study to examine the behaviour of the streamwise vortex structures in the near-field of a small-aspect-ratio ($\mathrm{AR} = 9$) stack, for a range of jet-to-cross-flow velocity ratios.

2. Experimental approach

The experimental set-up (Fig. 2) was similar to that adopted by Adaramola et al. (2007). The experiments were conducted in a low-speed, closed-return wind tunnel with a test-section of 0.91 m (height) × 1.13 m (width) × 1.96 m

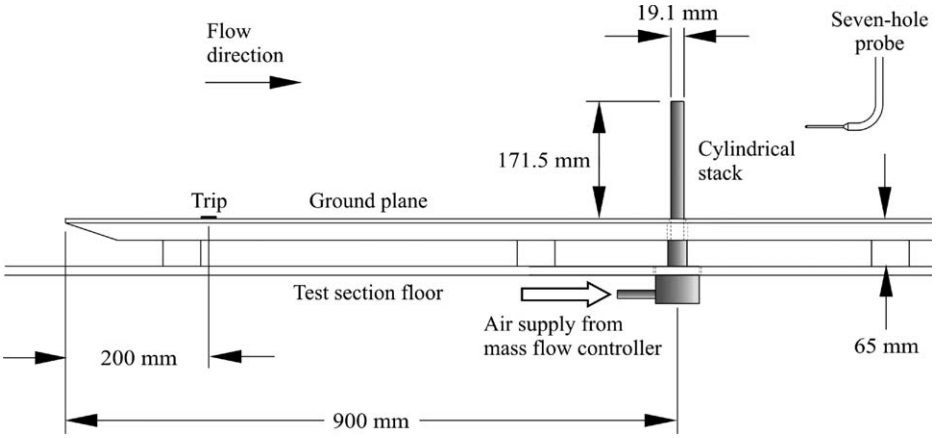

Fig. 2. Experiment set-up in the wind tunnel for the stack experiments.

(length). The longitudinal freestream turbulence intensity was less than 0.6% and the velocity non-uniformity outside the test-section wall boundary layers was less than 0.5%. The test-section floor was fitted with a ground plane. A roughness strip located about 200 mm from leading edge of the ground plane was used to enhance the development of a turbulent boundary layer on the ground plane at the location of the stack.

2.1. Experimental apparatus

A cylindrical stack of $H = 171.5$ mm, $D = 19.1$ mm, $d/D = 0.67$, and AR = 9, was used in the present study. This aspect ratio exceeds the critical aspect ratio for a finite circular cylinder, meaning that the stack is sufficiently slender for Kármán vortex shedding, and is consistent with the range of aspect ratios (AR = 8–25) used in other studies from the literature.

The experiments were conducted at a freestream velocity of $U_\infty = 20$ m/s, giving a Reynolds number, based on the stack external diameter, of $\mathrm{Re}_D = 2.3 \times 10^4$. The stack was located 700 mm downstream of the rough strip on the ground plane. At the location of the stack, the turbulent boundary layer on the ground plane provided a thickness-to-height ratio of $\delta/H \approx 0.5$ and the Reynolds number based on the boundary layer momentum thickness, θ, was $\mathrm{Re}_\theta = 0.86 \times 10^4$.

The air exiting the stack was unheated. A pair of screens was installed at the stack supply inlet to ensure the flow exiting the stack was turbulent. The exhaust velocity of the non-buoyant stack jet was varied with two MKS 1559A-200L mass flow controllers arranged in parallel. The jet-to-cross-flow velocity ratio was varied from $R = 0$ (no jet exiting the stack, i.e., a finite circular cylinder) to $R = 3$. The jet Reynolds number (based on the internal diameter of the stack and the average jet exit velocity) for the minimum exit velocity, when $R = 0.5$, was $\mathrm{Re}_d = 7.6 \times 10^3$, and for the maximum exit velocity, when $R = 3$, was $\mathrm{Re}_d = 4.7 \times 10^4$. The mean axial velocity profiles measured at a distance of $1d$ from the stack exit were similar to the typical velocity profile for a turbulent pipe flow [see Adaramola et al. (2007)].

2.2. Measurement instrumentation

The wind tunnel data were acquired with a personal computer, a National Instruments PCI-6031E 16-bit data acquisition card, and LabVIEW software. The freestream conditions were obtained with a Pitot-static probe (United Sensor, 3.2 mm diameter), Datametrics Barocel absolute and differential pressure transducers, and an Analog Devices AD590 integrated circuit temperature transducer. Data were sampled at 500 Hz for a period of 20 s.

Wake measurements were made with a seven-hole pressure probe (3.45 mm diameter, 30° cone angle). The seven pressures were measured with a Scanivalve ZOC-17 pressure scanner. A BOC Edwards Barocel differential pressure transducer with a thermal base was used as a transfer standard for "online" calibration of the ZOC-17 during measurements. The probe was calibrated in situ using an automated variable-angle calibrator, with a calibration grid spacing of 8.1° over a flow angle range of $\pm 72.9°$. A direct-interpolation calibration data-reduction method was used (Sumner, 2002). The measurement uncertainty was estimated to be less than 3° for the flow angle and less than 5% for the velocity magnitude.

The seven-hole probe was mounted in a three-axis, computer-controlled probe traversing system. For each value of R, the time-averaged wake velocity field (velocity components u, v, w, in the streamwise (x), cross-stream (y), and wall-normal (z) directions, respectively) was measured with the seven-hole probe on a 5 mm uniform grid. Measurements were made in a vertical (x–z) plane along the wake centreline (at $y/D = 0$) and in vertical (y–z) planes normal to the streamwise direction for $x/D = 6$–10.

From the velocity fields normal to the streamwise direction, the time-averaged streamwise vorticity field, $\omega_x(y, z)$, was determined using a first-order central-difference approach. In order to determine the circulation of the vortex structures and the vortex area, a vorticity cut-off of $\omega_x{}^* = 0.04$ (where $\omega_x{}^* = \omega_x D/U_\infty$) was used as a minimum vorticity level, similar to the approach used by Sumner et al. (2004); $\omega_x{}^* = 0.04$ was found to be the smallest contour value that sensibly and meaningfully defined the vortices, and corresponded to about 10% of the maximum vorticity encountered in all of the experiments. The size of the vortex was then determined by identifying connected regions of like-sign vorticity that exceed the minimum level. Similarly, the total circulation (or strength), Γ, for each vortex structure was found by summation of the vorticity greater than the cut-off value of $\omega_x{}^* = 0.04$ comprising the vortex [again, similar to Sumner et al. (2004)].

3. Results and discussion

Based on the previous study by Adaramola et al. (2007), which examined the turbulent velocity field behind the stack using hot-wire anemometry, the stack flow field can be broadly classified into three flow regimes depending on the value of the jet-to-cross-flow velocity ratio, R. In the present study, which was conducted at seven different velocity ratios, $R = 0$ and 0.5 corresponded to the downwash flow regime, $R = 1$ corresponded to the crosswind-dominated flow regime, and $R = 1.5$, 2, 2.5, and 3 corresponded to the jet-dominated flow regime.

3.1. Velocity vector fields in planes on the wake centreline

The time-averaged velocity fields measured in vertical planes situated on the stack wake centreline ($y/D = 0$) are shown in Figs. 3–5 for the three different flow regimes. In these figures, the blank space behind the stack (where there is an absence of velocity vectors) indicate the region where the flow exceeded the angular range of the seven-hole probe (Sumner, 2002; Sumner et al., 2004), which was estimated at $\pm 70^\circ$. Much of the flow in these blank regions will also be reversing, and therefore the blank regions can be broadly interpreted as, or can approximately represent, the recirculation zones behind the stack and jet. The details of the flow within these blank regions, i.e., within the near-wake of the stack and about the immediate vicinity of the free end and the jet exit, have already been reported in other studies in the literature. For instance, Huang and Hsieh (2002, 2003) used flow visualization and laser Doppler velocimetry (LDV) to study the near-wake of a stack for $x/D < 10$, focusing on the topology of the flow patterns on the vertical symmetry plane. Also, Mahjoub Saïd et al. (2005, 2007) used numerical modelling, particle image velocimetry (PIV) and laser tomography visualization to study the near-wake of a stack for $x/D < 7$.

When $R = 0$ (Fig. 3(a)), which corresponds to the case of the finite circular cylinder (no jet flow exiting the stack), strong downwash flow (downward-directed velocity vectors) occurs within the near-wake of the stack. The downwash originates near the free end and extends downwards towards the mid-height of the stack. An upwash flow (upward-directed velocity vectors) is observed near the ground plane and within the flat-plate boundary layer. These downwash and upwash flows are similar to the results for a finite circular cylinder, as reported by Tanaka and Murata (1999) for AR = 10 and Sumner et al. (2004) and Adaramola et al. (2006) for AR ≥ 5. The streamwise extent of the region of recirculating flow (the blank region without velocity vectors) varies along the stack height, with its maximum length occurring near mid-height. Finite circular cylinder experiments have shown that as the cylinder aspect ratio increases, the maximum streamwise extent of this region decreases and approaches the size observed for an infinite cylinder [e.g., Okamoto (1991); Tanaka and Murata (1999); Sumner et al. (2004)].

In the case of $R = 0.5$ (Fig. 3(b)), which corresponds to the downwash flow regime (weak jet flow exiting the stack), downwash continues to be observed within the stack wake near the free end, and upwash flow is observed near the ground plane and within the ground plane boundary layer. The flow pattern is similar to the finite-cylinder case, when $R = 0$ (Fig. 3(a)), but the strength of the downwash flow, and the streamwise and vertical extent of the upwash flow, are both smaller. In addition, for $R = 0.5$, the streamwise extent of the recirculation region is smaller and extends more toward the stack free end. This may be due to the presence of the weak jet flow, which reduces the downwash flow into the stack wake but is not strong enough to prevent it entirely. The experiments by Huang and Hsieh (2002, 2003) for $R = 0.1$ and 0.43, $\mathrm{Re}_D = 2074$, and AR = 25, showed that a portion of the downwash flow recirculates upstream and

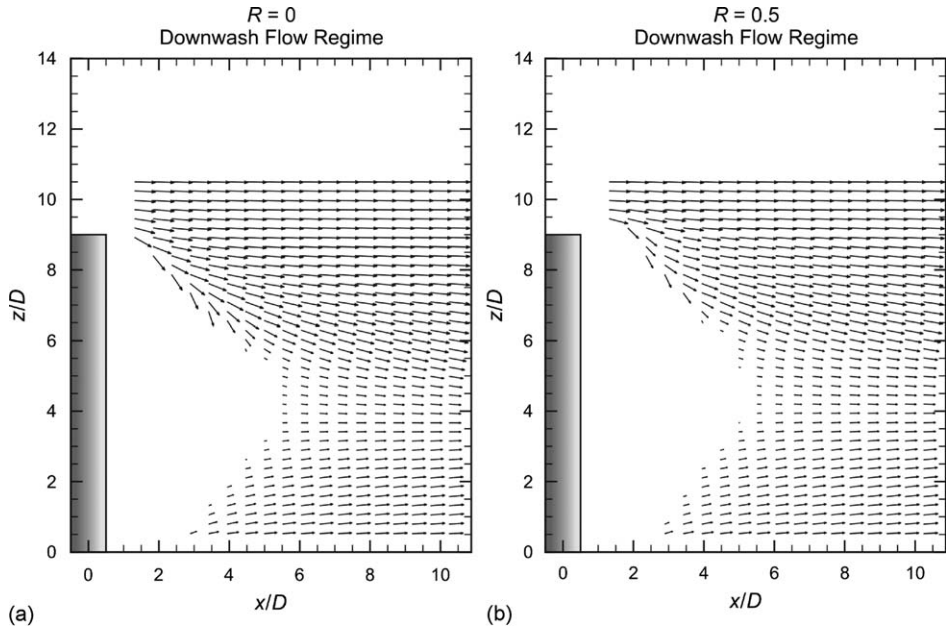

Fig. 3. The time-averaged velocity field along the wake centreline (u, w velocity components, measured in a vertical plane at $y/D = 0$) for the *downwash flow regime*: (a) $R = 0$, (b) $R = 0.5$.

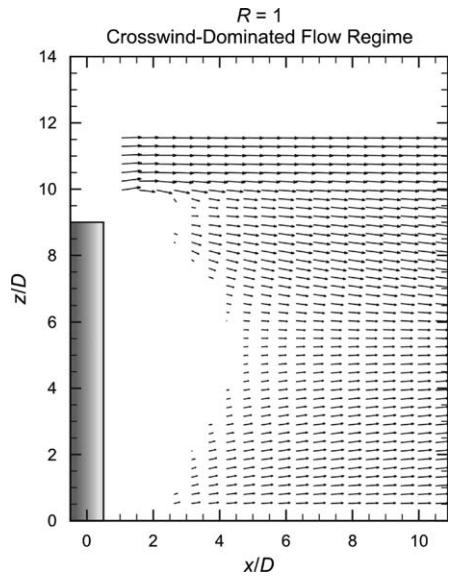

Fig. 4. The time-averaged velocity field along the wake centreline (u, w velocity components, measured in a vertical plane at $y/D = 0$) for the *crosswind-dominated flow regime*, $R = 1$.

appears to stagnate on the rear surface of the stack. This behaviour of the near-wake recirculation zone was confirmed in the experiments of Mahjoub Saïd et al. (2007), for $R = 0.5$, $\mathrm{Re}_D = 5330$, and $\mathrm{AR} = 8.3$.

For the crosswind-dominated flow regime, shown for $R = 1$ in Fig. 4, the downwash flow is absent in the near-wake of the stack. The streamwise extent of the upwash flow and the recirculation region within the stack wake are now smaller compared with the downwash flow regime (Fig. 3(b)). Another recirculation region (again, denoted by the blank region with the absence of velocity vectors) is also observed above the free end of the stack and within the jet wake (extending to $x/D = 3$). This region may contain the jet-wake vortex (with axis normal to the vertical plane) observed by

Huang and Hsieh (2002) for $0.95 < R < 2.4$, which they reported to be the result of "interaction between the jet shear layer and downwash flow." From the experiments of Mahjoub Saïd et al. (2007) at $R = 1$ and $\mathrm{Re} = 5330$, this vortex was less apparent and the flow immediately behind the stack was mostly stagnant.

In the case of the jet-dominated flow regime, when $R \geq 1.5$ (Fig. 5), the stronger momentum of the jet flow allows it to penetrate deeper into the cross-flow, as shown by the strong upward-directed velocity vectors above the free end of the stack. The increasing strength of the jet is evident as the velocity ratio increases from $R = 1.5$ (Fig. 5(a)) to $R = 3$ (Fig. 5(d)). With the increased jet rise, the recirculation region within the jet wake is now larger compared to the crosswind-dominated flow regime at $R = 1$ (Fig. 4). A strong recirculation region within the jet wake was also observed by Mahjoub Saïd et al. (2005, 2007). With increasing R, there is also a corresponding reduction in the size of the

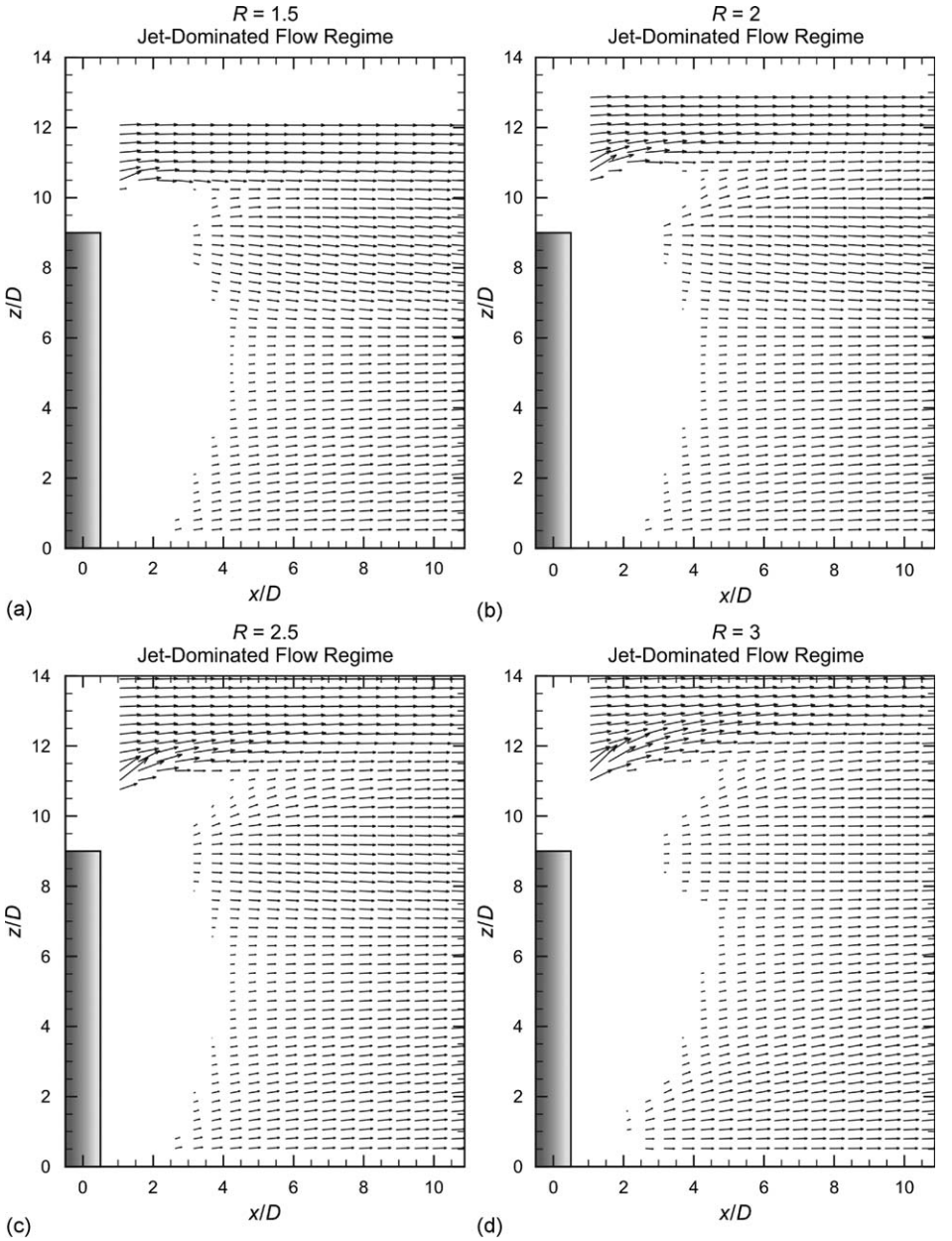

Fig. 5. The time-averaged velocity field along the wake centreline (u, w velocity components, measured in a vertical plane at $y/D = 0$) for the *jet-dominated flow regime*: (a) $R = 1.5$; (b) $R = 2$; (c) $R = 2.5$; (d) $R = 3$.

recirculation region within the stack wake, and the streamwise extent of this region becomes shorter and more uniform along the stack height. The experiments by Mahjoub Saïd et al. (2007) showed the mean flow within the stack near-wake region to be more disorderly. With the increase in momentum of the jet, therefore, the stack wake becomes closer to that of an infinite circular cylinder; in other words, the presence of the jet flow increases the effective aspect ratio of the stack (Adaramola et al., 2007).

3.2. Velocity vector and vorticity fields in planes normal to the streamwise direction

The time-averaged velocity fields measured in vertical planes normal to the streamwise direction (v, w velocity components, measured in the y–z plane) are presented in the upper parts of Figs. 6–12. Shown in the lower parts of Figs. 6–12 are the corresponding time-averaged streamwise vorticity (ω_x*) fields. The vorticity is presented as a contour plot, where the solid contour lines represent positive (CCW) vorticity and the dashed contour lines represent negative (CW) vorticity. Results are shown for two or three streamwise positions (x/D), depending on the value of R. In these figures, the minimum vorticity contour shown corresponds to a magnitude of $\omega_x^* = 0.04$.

For all of the velocity ratios ($R = 0$–3, Figs. 6–12), the velocity vector fields show an upwash flow within the flat-plate boundary layer on the ground plane. The upwash strength is strongest within the flat-plate boundary layer on the ground plane and reduces towards the mid-height of the stack. The upwash flow weakens with increasing streamwise distance (x/D) from the stack.

3.2.1. Downwash flow regime

For the downwash flow regime (Figs. 6 and 7, for $R = 0$ and 0.5, respectively), the velocity vector fields show the presence of a strong downwash flow within the stack wake and below the stack free end. The strength of the downwash flow reduces along the height of the stack when moving away from the free end and towards the ground plane. There are also two counter-rotating vortex pairs within the stack wake: one pair near the stack free end, referred to as the "tip vortex pair", and another of opposite sense of rotation closer to the base of the stack, referred to as the "base vortex pair." These two pairs of vortex structures are evident in the time-averaged cross-stream velocity vector fields, and are also observed in the wake of a finite circular cylinder (Tanaka and Murata, 1999; Sumner et al., 2004; Wang et al., 2006).

Similar to the case of the finite circular cylinder, the tip vortex pair and the base vortex pair are associated with the downwash velocity along the wake centreline behind the free end of the stack (as shown in the vortex pair model described by Johnston and Wilson (1997)) and the upwash velocity within the plane-wall boundary layer close to the ground plane, respectively. The region on the wake centreline behind the cylinder, centred between the four vortex centres, where the upwash and downwash flows meet and interact, is also known to be an area of elevated streamwise and wall-normal turbulence intensity (Adaramola et al., 2007).

The tip vortex structures may represent the Kármán vortex axes that have been bent towards the tip, where a larger portion of the vorticity is in the streamwise direction, while the base vortex structures may represent the same Kármán vortex axes as they bend towards the cylinder–wall junction. The tip vortices may also be distinct vortex structures that have their origin near the free end of the stack, similar to what was depicted by Kawamura et al. (1984). Nonetheless, a definitive physical interpretation of these vortex structures remains lacking in the literature.

For $R = 0$ (Fig. 6), the tip vortex pair at $x/D = 6$ is located below the free end. This is similar to the observations of Tanaka and Murata (1999) and Sumner et al. (2004) for a finite circular cylinder. For $R = 0.5$ (Fig. 7), the tip vortex pair moves toward the free end of the stack but still lies within the stack wake. In addition, the base vortex structures become stretched in the vertical direction, but remain within the turbulent boundary layer on the ground plane.

3.2.2. Crosswind-dominated flow regime

For the crosswind-dominated flow regime (Fig. 8, $R = 1$), the velocity vector fields show that the downwash velocity field is located further away from the ground plane and closer to the stack's free end. The downwash flow is weaker than for $R = 0.5$ (Fig. 7). There are still two counter-rotating vortex pairs within the stack wake. However, the tip vortex pair (which is associated with the downwash flow field) now extends above the free end while for $x/D = 6$ (Fig. 8(a)) the base vortex structures (which are associated with the upwash flow field) are stretched upward along the sides of the stack towards the mid-height position. At $x/D = 10$ (Fig. 8(b)), the base vortex structures are still confined to the boundary layer on the ground plane. The region centred between the four vortex centres continues to be an area of elevated turbulence intensity (Adaramola et al., 2007).

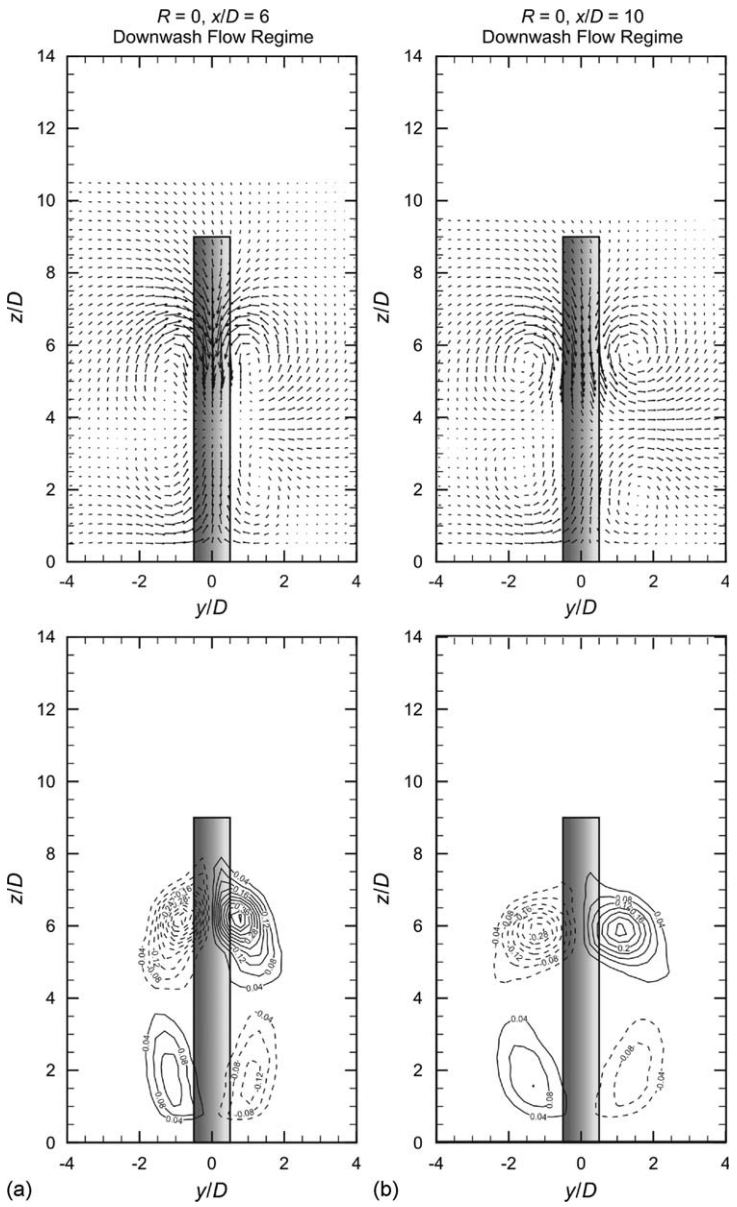

Fig. 6. The time-averaged velocity vector field (v, w components) and streamwise vorticity field (ω_x*) downstream of the stack for $R = 0$ (downwash flow regime) measured in a vertical plane at (a) $x/D = 6$ and (b) $x/D = 10$. For the vorticity fields: solid contour lines represent positive (CCW) vorticity; dashed contour lines represent negative (CW) vorticity; minimum vorticity contour of $\omega_x^* = \pm 0.04$; contour increment of $\Delta\omega_x^* = 0.04$.

3.2.3. *Jet-dominated flow regime*

For the jet-dominated flow regime (Figs. 9–12, for $R = 1.5$, 2.0, 2.5, and 3, respectively), another and much stronger upwash flow, related to the rise of the jet, occurs above the free end of the stack within the jet-wake region. This upwash flow extends more than two to four stack diameters above the stack tip, depending on R. In contrast, the downwash becomes weaker with increasing R, and effectively disappears at $R = 3$ (Fig. 12). The vorticity fields now show a third counter-rotating vortex pair, found within the jet-wake region, in addition to the tip vortex and base vortex pairs. This third vortex pair is clearly associated with the rise of the jet and the additional upwash velocity field noted above. From Adaramola et al. (2007), changes also occur in the streamwise and wall-normal turbulence intensity fields, and in the behaviour of the streamwise-wall-normal Reynolds shear stress field.

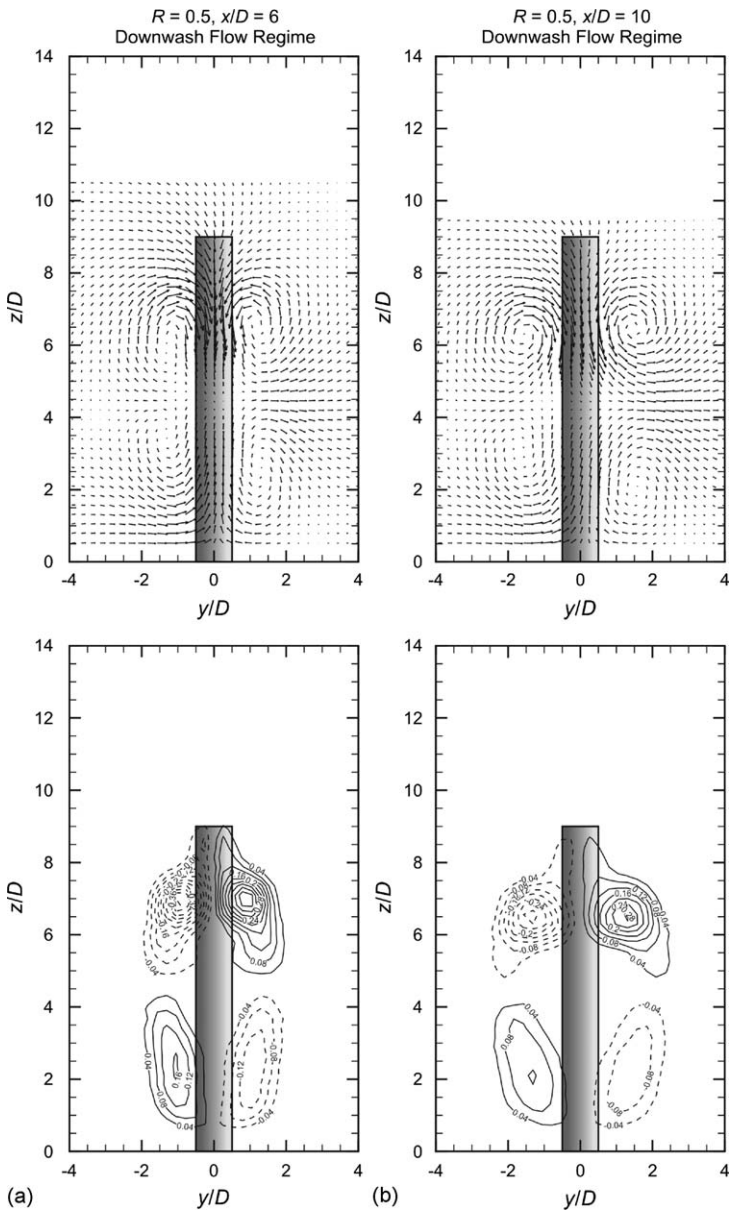

Fig. 7. The time-averaged velocity vector field (v, w components) and streamwise vorticity field (ω_x*) downstream of the stack for $R = 0.5$ (downwash flow regime) measured in a vertical plane at (a) $x/D = 6$ and (b) $x/D = 10$. For the vorticity fields: solid contour lines represent positive (CCW) vorticity; dashed contour lines represent negative (CW) vorticity; minimum vorticity contour of $\omega_x^* = \pm 0.04$; contour increment of $\Delta\omega_x^* = 0.04$.

The base vortex structures remain stretched along the height of the stack, similar to the crosswind-dominated flow regime; for $R = 1.5$–2.5, at $x/D = 10$, these vortices remain within the boundary layer on the ground plane. Quite the opposite, the tip vortex structures are reduced in size within the jet-dominated flow regime and almost disappear when $R = 3$ (Fig. 12); this is consistent with the weakening of the downwash phenomenon. The third vortex pair, referred to as the "jet-wake vortex pair", has the opposite sense of rotation to the tip vortex pair. The jet-wake vortex structures are stronger than the tip vortex structures. A saddle point may be distinguished in the velocity vector field in the jet-wake region on the wake centreline, where the v and w velocity components are zero. This saddle point separates the tip and jet-wake counter-rotating vortex pairs. The location of this saddle point within the jet wake and above the stack free end is observed to be slightly elevated with increasing R (Figs. 9–12), and disappears when $R = 3$ (Fig. 12).

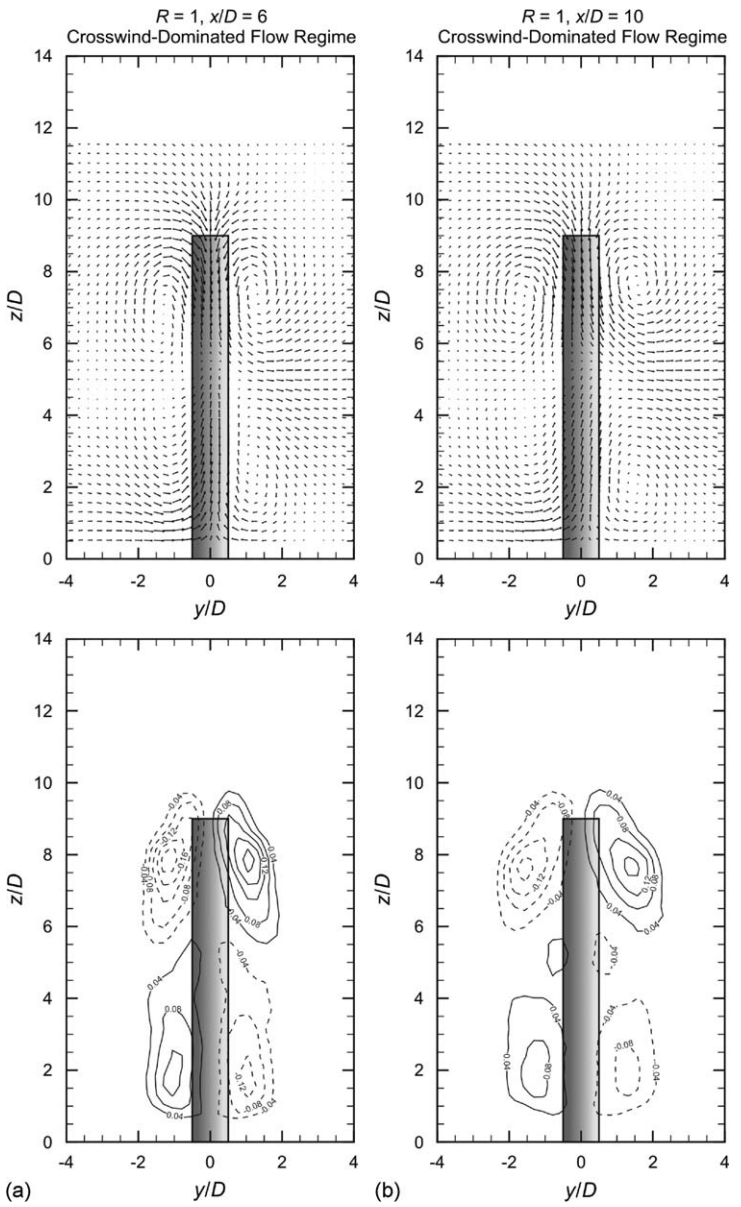

Fig. 8. The time-averaged velocity vector field (v, w components) and streamwise vorticity field (ω_x*) downstream of the stack for $R = 1$ (crosswind-dominated flow regime) measured in a vertical plane at (a) $x/D = 6$ and (b) $x/D = 10$. For the vorticity fields: solid contour lines represent positive (CCW) vorticity; dashed contour lines represent negative (CW) vorticity; minimum vorticity contour of $\omega_x^* = \pm 0.04$; contour increment of $\Delta\omega_x^* = 0.04$.

The jet-wake vortex structures are associated with the jet rise, and therefore their size and strength increase with R, similar to the observation of Plesniak and Cusano (2005) for a ground-level source jet flow. The jet rise is evident in the locations of the solid black dots in Figs. 9–12, which represent the locations of the maximum jet centreline velocity; these locations occur farther away from the ground plane at $x/D = 10$ compared with $x/D = 6$.

3.3. Properties of the streamwise vortex structures

The values of the peak streamwise vorticity (ω_x) and vortex strength (circulation, Γ) of the base vortex, tip vortex and the jet-wake vortex structures are shown in Fig. 13 for $x/D = 6$ and 10 as a function of R (note that the jet vortex

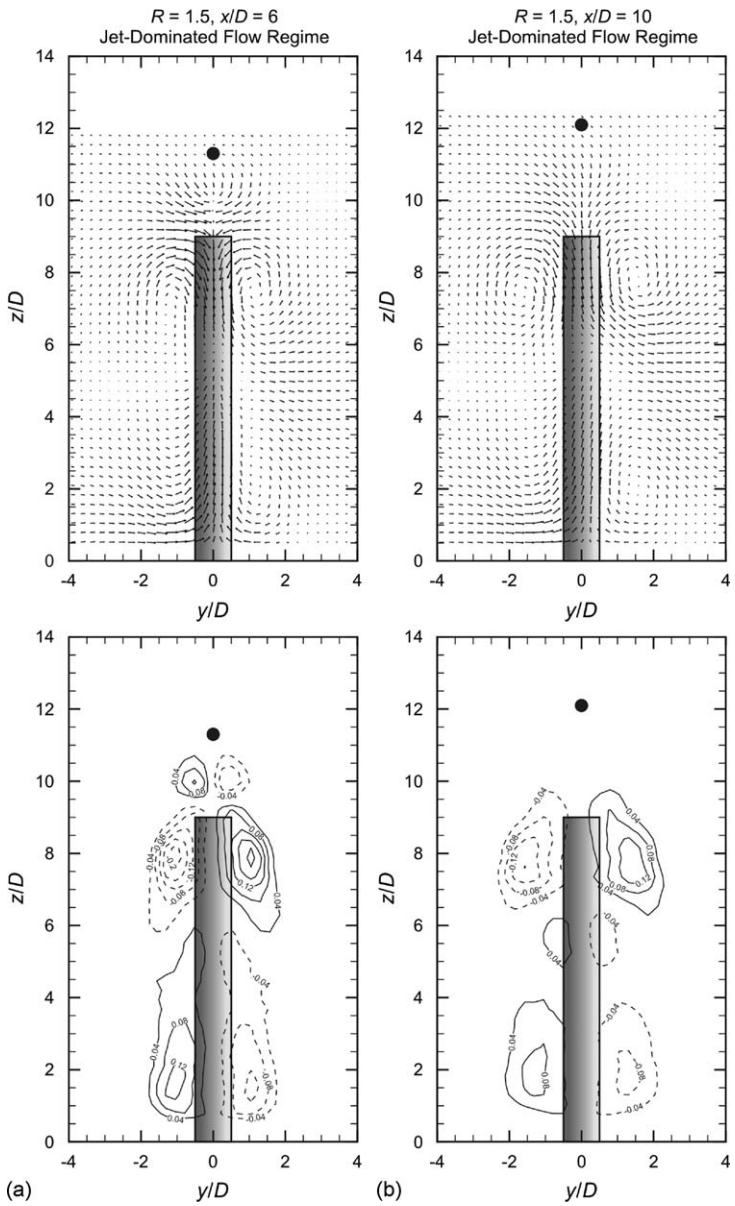

Fig. 9. The time-averaged velocity vector field (v, w components) and streamwise vorticity field (ω_x*) downstream of the stack for $R = 1.5$ (jet-dominated flow regime) measured in a vertical plane at (a) $x/D = 6$ and (b) $x/D = 10$. The black dot represents the jet flow trajectory point. For the vorticity fields: solid contour lines represent positive (CCW) vorticity; dashed contour lines represent negative (CW) vorticity; minimum vorticity contour of $\omega_x^* = \pm 0.04$; contour increment of $\Delta\omega_x^* = 0.04$.

structures only exist for $R \geq 1.5$). The data shown in Fig. 13 represent an average of the vortices on either side of the wake centreline. The general trend is for both the peak streamwise vorticity and the strength of the streamwise vortex structures to decrease with increasing streamwise distance (x/D) from the stack. The tip vortex structures are more strongly affected by the velocity ratio, compared to the base vortex structures, since they originate near the free end of the stack where the interaction between the jet, cross-flow, and wake is the strongest. Furthermore, the tip vortices are closely associated with the downwash phenomenon, which itself diminishes with increasing velocity ratio. In contrast, the upwash within the boundary layer on the ground plane is relatively insensitive to the velocity ratio (as seen in the earlier figures); hence, the properties of the base vortices (which are associated with the upwash) remain relatively unaffected. It is noted that changes in the properties of the streamwise vortex structures with x/D and/or R may be

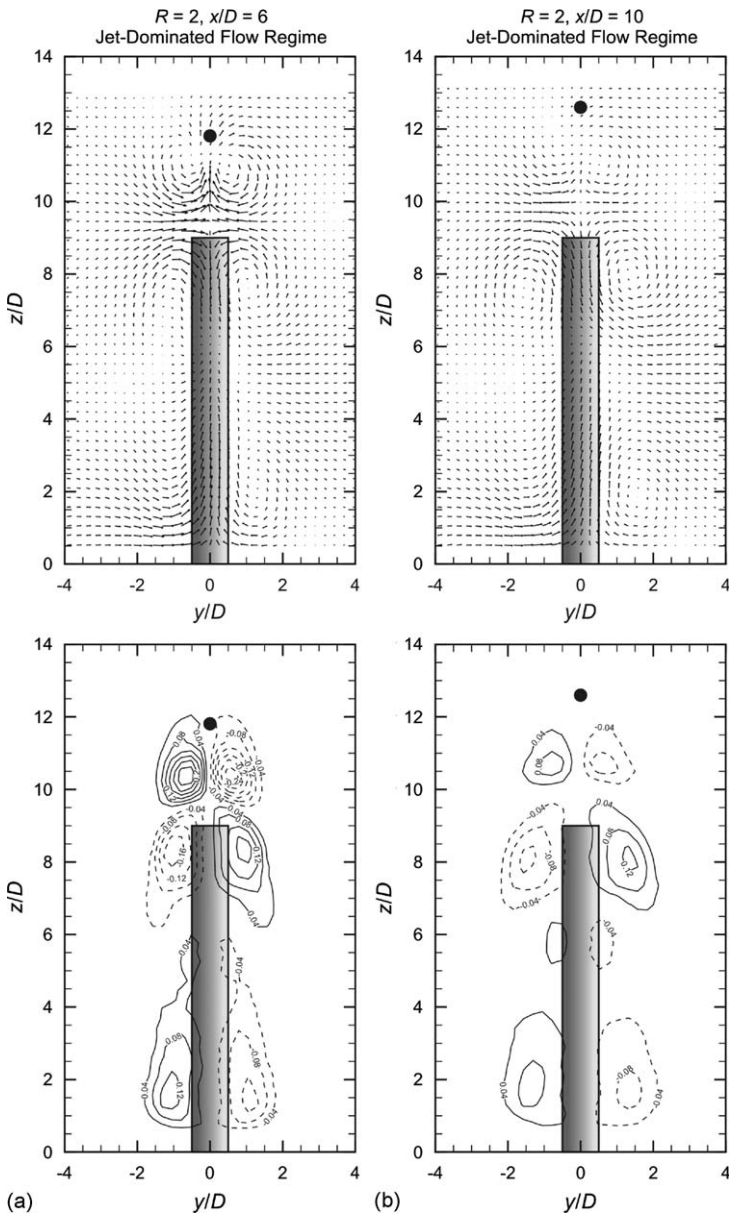

Fig. 10. The time-averaged velocity vector field (v, w components) and streamwise vorticity field (ω_x*) downstream of the stack for $R = 2$ (jet-dominated flow regime) measured in a vertical plane at (a) $x/D = 6$ and (b) $x/D = 10$. The black dot represents the jet flow trajectory point. For the vorticity fields: solid contour lines represent positive (CCW) vorticity; dashed contour lines represent negative (CW) vorticity; minimum vorticity contour of $\omega_x^* = \pm 0.04$; contour increment of $\Delta\omega_x^* = 0.04$.

attributed to several factors, including the redistribution of streamwise vorticity to other coordinate directions (cross-stream or wall-normal vorticity components, neither of which were measured in the present experiments), the diffusion of vorticity due to turbulence, dissipation of vorticity, or the cancellation of vorticity due to vorticity of opposite sign.

At a given streamwise location, x/D, the peak streamwise vorticity (Fig. 13(a)) of the base vortex structures stays relatively independent of R. For the tip vortex structures, at a given x/D, the peak streamwise vorticity value decreases as R increases. This reduction in peak vorticity coincides with the reduction in the strength of the downwash flow from the stack free end, the downwash resulting from the interaction of the two counter-rotating streamwise vortices

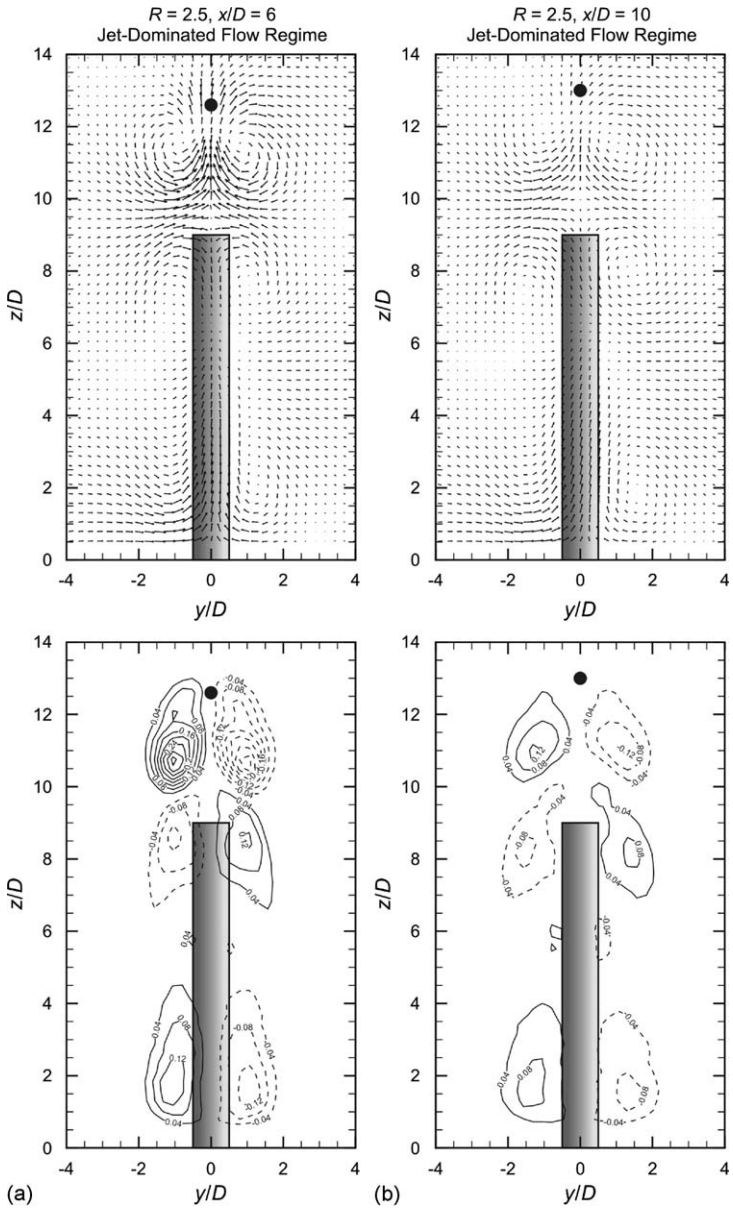

Fig. 11. The time-averaged velocity vector field (v, w components) and streamwise vorticity field (ω_x*) downstream of the stack for $R = 2.5$ (jet-dominated flow regime) measured in a vertical plane at (a) $x/D = 6$ and (b) $x/D = 10$. The black dot represents the jet flow trajectory point. For the vorticity fields: solid contour lines represent positive (CCW) vorticity; dashed contour lines represent negative (CW) vorticity; minimum vorticity contour of $\omega_x^* = \pm 0.04$; contour increment of $\Delta\omega_x^* = 0.04$.

comprising the pair (Johnston and Wilson, 1997; Sumner et al., 2004). In contrast, the peak streamwise vorticity value of the jet vortex structures increases with R; this coincides with an increase in the momentum of the jet exiting the stack.

The vortex strength or circulation (Fig. 13(b)) data at $R = 0$ (where there is no jet exiting the stack, corresponding to the case of the finite circular cylinder) are similar to those from Sumner et al. (2004), despite the differences in Reynolds number and δ/H. The base vortex strength at $x/D = 6$ increases gradually from $R = 0$ (downwash flow regime) to $R = 3$ (jet-dominated flow regime). A little farther from the stack, at $x/D = 10$, however, the base vortex strength shows less sensitivity to R. The tip vortex strength decreases as R increases, with the largest decrease occurring when moving from

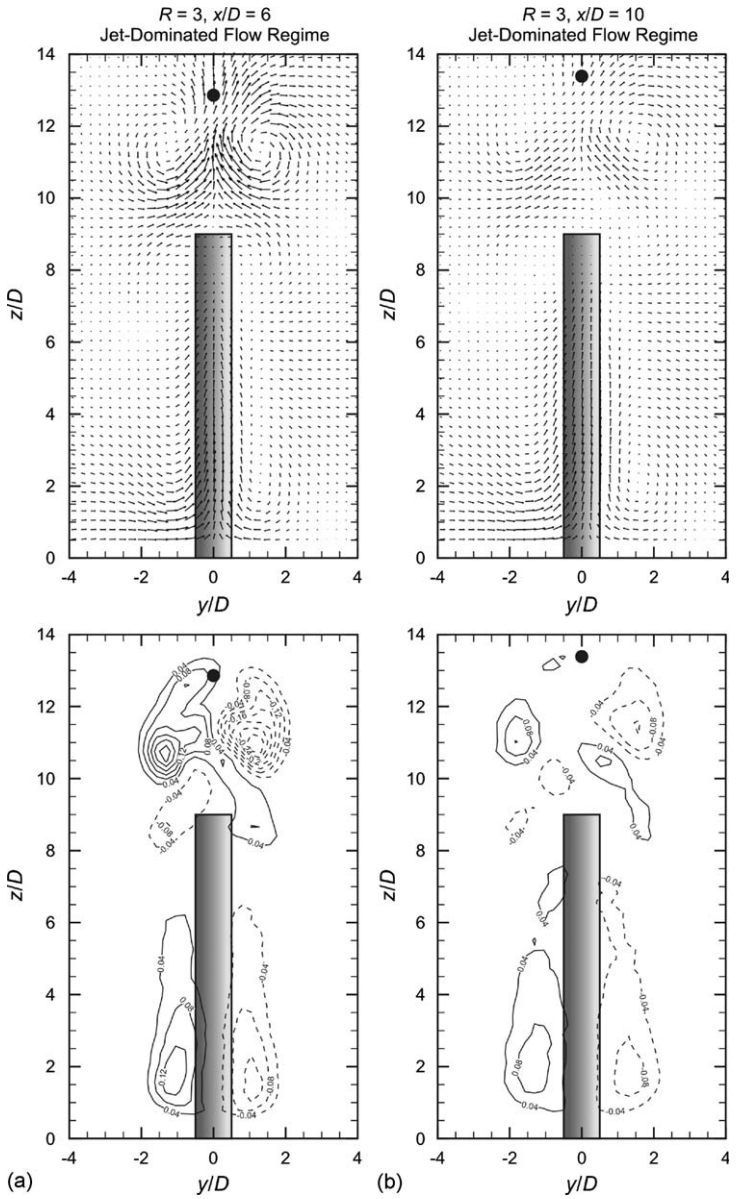

Fig. 12. The time-averaged velocity vector field (v, w components) and streamwise vorticity field (ω_x*) downstream of the stack for $R = 3$ (jet-dominated flow regime) measured in a vertical plane at (a) $x/D = 6$ and (b) $x/D = 10$. The black dot represents the jet flow trajectory point. For the vorticity fields: solid contour lines represent positive (CCW) vorticity; dashed contour lines represent negative (CW) vorticity; minimum vorticity contour of $\omega_x^* = \pm 0.04$; contour increment of $\Delta\omega_x^* = 0.04$.

the downwash and crosswind-dominated flow regimes ($R \leq 1$) to the jet-dominated flow regime ($R > 1$). Similar to the peak vorticity values, the strength of the jet vortex structures increases with R.

4. Conclusions

In the present study, a seven-hole pressure probe was used to measure the time-averaged velocity and streamwise vorticity fields in the wake of a stack operating at jet-to-cross-flow velocity ratios ranging from $R = 0$ to 3 at a stack Reynolds number of $\mathrm{Re}_D = 2.3 \times 10^4$. The stack, of aspect ratio $\mathrm{AR} = 9$, was mounted normal to a ground plane and

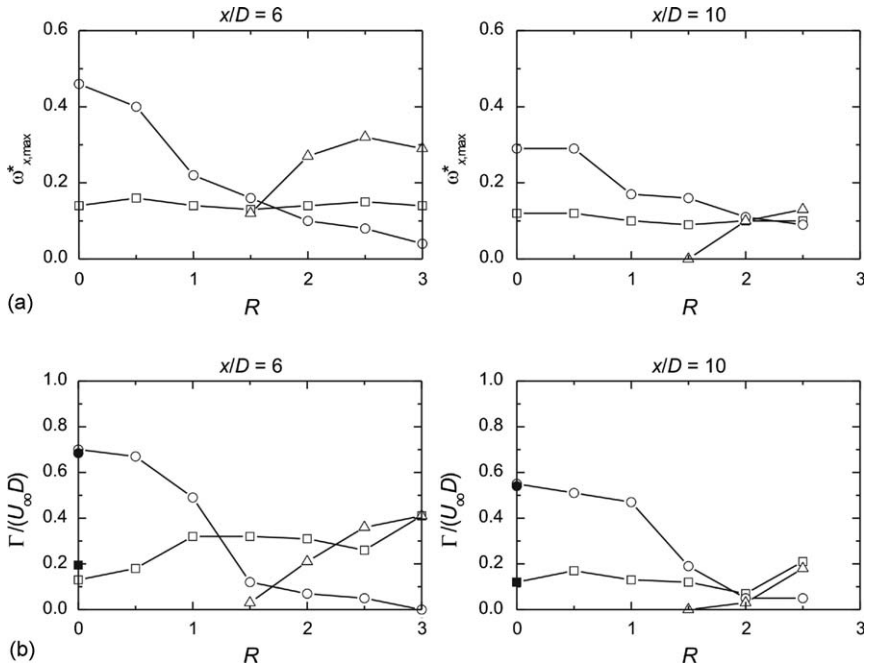

Fig. 13. Time-averaged properties of the streamwise vortex structures at $x/D = 6$ and $x/D = 10$: (a) peak streamwise vorticity; (b) vortex strength (circulation). Stack (current study): □, base vortex structures; ○, tip vortex structures; △, jet-wake vortex structures. Finite circular cylinder (Sumner et al., 2004), AR = 9, $Re_D = 6 \times 10^4$, $\delta/H = 0.3$: ■, base vortex structures; ●, tip vortex structures.

was partially immersed in a flat-plate turbulent boundary layer, where the ratio of the boundary layer thickness to the stack height was $\delta/H \approx 0.5$. The range of velocity ratio covered three main flow regimes describing the fluid behaviour close to the stack, namely the downwash, crosswind-dominated, and jet-dominated flow regimes. As R is varied, marked changes occur in the downwash velocity field, the location, strength, and number of counter-rotating streamwise vortex pairs, and the size and shape of the recirculation zone in the near-wake of the stack.

In the downwash flow regime ($R < 0.7$), the flow is similar to that of a finite circular cylinder, with two pairs of counter-rotating streamwise vortex structures in the stack wake. The tip vortex pair is found closer to the free end of the stack and is associated with a strong downwash velocity field immediately behind the stack. The weaker base vortex pair is found within the boundary layer on the ground plane and is associated with an upwash velocity field directed away from the ground plane.

In the crosswind-dominated flow regime ($0.7 \leq R < 1.5$), the tip vortex pair is located just above the free end of the stack and the base vortex pair becomes stretched vertically towards the mid-height of the stack. The downwash velocity field and the associated tip vortex pairs are weakened compared to the downwash flow regime.

For the jet-dominated flow regime ($R \geq 1.5$), three pairs of counter-rotating streamwise vortex structures are observed. In addition to the tip vortex and base vortex pairs found at lower velocity ratios, the jet-wake vortex pair appears in the jet-wake region above the free end of the stack. The jet-wake vortex pair is associated with the jet rise and a strong upwash velocity on the jet wake centreline.

Based on the results of the present study, a schematic of the flow field for the jet-dominated flow regime is presented in Fig. 14, which shows the three main types of time-averaged streamwise vortex pairs. Also shown in Fig. 14 are the other main wake vortex flow patterns, namely Kármán vortex shedding from the main body of the stack [discussed in more detail in the earlier study by Adaramola et al. (2007)] and the horseshoe vortex which forms at the stack-wall junction (which has received extensive treatment elsewhere in the literature). For the downwash and crosswind-dominated flow regimes, for which the jet-wake vortex pair is absent, the proposed model of the wake flow is consistent with the wake vortex flow patterns described by Kawamura et al. (1984) (for finite cylinders greater than the critical aspect ratio) and the tip-vortex-downwash model proposed by Johnston and Wilson (1997). For the jet-dominated regime, the appearance of the jet-wake vortex pair in the schematic is consistent with the jet-wake vortex flow patterns proposed by Eiff and Keffer (1997).

The schematic in Fig. 14 is an attempt to summarize the main flow features identified in the present study, and, taken together with the other models proposed in the literature, is another step towards developing a comprehensive physical

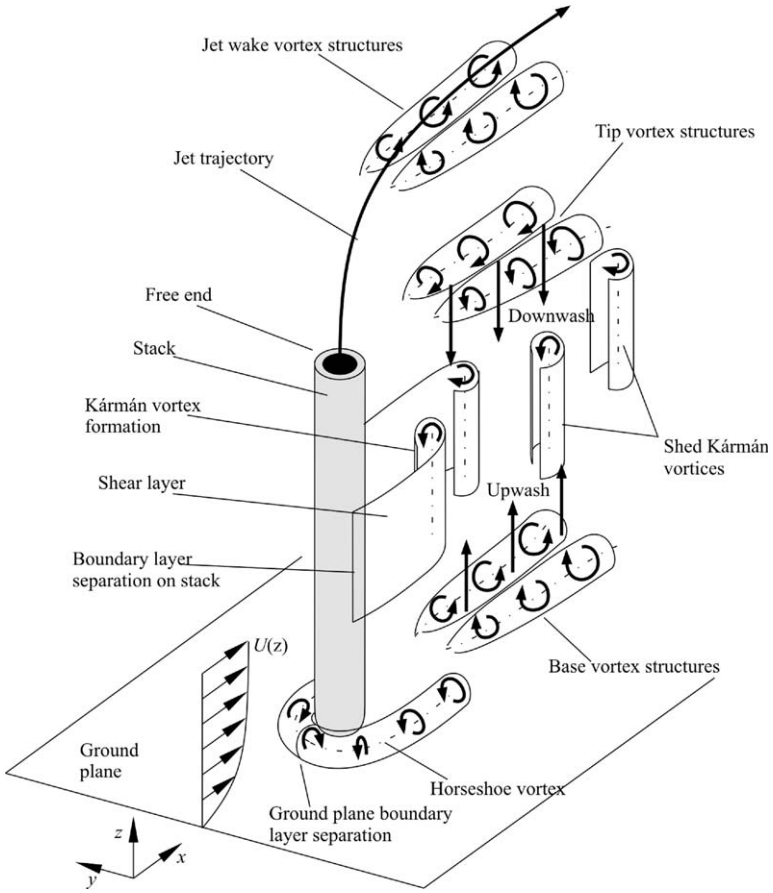

Fig. 14. Schematic of the flow behind a stack operating in the jet-dominated flow regime, based on the results of the present study, showing the main time-averaged streamwise vortex structures.

explanation of the behaviour of the flow around a stack. The exact behaviour of the streamwise vortex structures close to the stack, i.e. in the vicinity of the recirculation zone and near the free end, and the interactions between the streamwise vortex structures and the Kármán vortices, remain ambiguous (even for the simpler case of the finite circular cylinder), and are absent in the model shown in Fig. 14. The relationship, if any, between the streamwise vortex pairs and the attached vortex structures near the free end and within the jet-wake region, which were documented by Huang and Hsieh (2002, 2003), is uncertain. Also, synchronization of the Kármán vortex structures in the stack wake region with similar vortex structures in the jet-wake region, observed by Eiff et al. (1995), Eiff and Keffer (1997, 1999), and Moussa et al. (1977), will need to be incorporated into a comprehensive model of the flow behaviour.

Acknowledgments

The authors acknowledge the financial support of the Natural Sciences and Engineering Research Council of Canada (NSERC), the Canada Foundation for Innovation (CFI), the Innovation and Science Fund of Saskatchewan, and the Division of Environmental Engineering. The assistance of D.M. Deutscher and Engineering Shops is appreciated.

References

Adaramola, M.S., Akinlade, O.J., Sumner, D., Bergstrom, D.J., Schenstead, A.J., 2006. Turbulent wake of a finite circular cylinder of small aspect ratio. Journal Fluids and Structures 22, 919–928.

Adaramola, M.S., Sumner, D., Bergstrom, D.J., 2007. Turbulent wake and vortex shedding for a stack partially immersed in a turbulent boundary layer. Journal of Fluids and Structures 23, 1189–1206.

Andreopoulos, J., Rodi, W., 1984. Experimental investigation of jets in a crossflow. Journal of Fluid Mechanics 138, 93–127.

Eiff, O.S., Kawall, J.G., Keffer, J.F., 1995. Lock-in of vortices in the wake of an elevated round turbulent jet in a crossflow. Experiments in Fluids 19, 203–213.

Eiff, O.S., Keffer, J.F., 1997. On the structures in the near-wake region of an elevated turbulent jet in a crossflow. Journal of Fluid Mechanics 333, 161–195.

Eiff, O.S., Keffer, J.F., 1999. Parametric investigation of the wake-vortex lock-in for the turbulent jet discharging from a stack. Experimental Thermal and Fluid Science 19, 57–66.

Fric, T.F., Roshko, A., 1994. Vortical structure in the wake of a transverse jet. Journal of Fluid Mechanics 279, 1–47.

Huang, R.F., Hsieh, R.H., 2002. An experimental study of elevated round jets deflected in a crossflow. Experimental Thermal and Fluid Science 27, 77–86.

Huang, R.F., Hsieh, R.H., 2003. Sectional flow structures in near wake of elevated jet in a crossflow. AIAA Journal 41, 1490–1499.

Johnston, C.R., Wilson, D.J., 1997. A vortex pair model for plume downwash into stack wakes. Atmospheric Environment 31, 13–20.

Kawamura, T., Hiwada, M., Hibino, T., Mabuchi, T., Kumada, M., 1984. Flow around a finite circular cylinder on a flat plate. Bulletin of the JSME 27, 2142–2150.

Lim, T.T., New, T.H., Luo, S.C., 2001. On the development of large-scale structures of a jet normal to a cross flow. Physics of Fluids 13, 770–775.

Mahjoub Saïd, N., Mhiri, H., Le Palec, G., Bournot, P., 2005. Experimental and numerical analysis of pollutant dispersion from a chimney. Atmospheric Environment 39, 1727–1738.

Mahjoub Saïd, N., Habil, S., Mhiri, H., Bournot, H., Le Palec, G., 2007. Flow field measurement in a crossflowing elevated jet. ASME Journal of Fluids Engineering 129, 551–562.

Moussa, Z.M., Trischka, J.W., Eskinazi, S., 1977. The near field in the mixing of a round jet with a cross-stream. Journal of Fluid Mechanics 80, 49–80.

New, T.H., Lim, T.T., Luo, S.C., 2006. Effects of jet velocity profiles on a ground jet in cross-flow. Experiments in Fluids 40, 859–875.

Okamoto, S., 1991. Flow past circular cylinder of finite length placed on ground plane. Transaction of the Japan Society for Aeronautical and Space Sciences 33, 234–246.

Overcamp, T.J., Ku, T., 1988. Plume rise from two or more adjacent stacks. Atmospheric Environment 22, 625–637.

Plesniak, M.W., Cusano, D.W., 2005. Scalar mixing in a confined rectangular jet in crossflow. Journal of Fluid Mechanics 524, 1–45.

Smith, S.H., Mungal, M.G., 1998. Mixing, structure and scaling of the jet in crossflow. Journal of Fluid Mechanics 357, 83–122.

Sumner, D., 2002. A comparison of data-reduction methods for a seven-hole probe. ASME Journal of Fluids Engineering 124, 523–527.

Sumner, D., Heseltine, J.L., Dansereau, O.J.P., 2004. Wake structure of a finite circular cylinder of small aspect ratio. Experiments in Fluids 37, 720–730.

Tanaka, S., Murata, S., 1999. An investigation of the wake structure and aerodynamic characteristics of a finite circular cylinder. JSME International Journal Series B: Fluids and Thermal Engineering 42, 178–187.

Wang, H.F., Zhou, Y., Chan, C.K., Lam, K.S., 2006. Effect of initial conditions on interaction between a boundary layer and a wall-mounted finite-length-cylinder wake. Physics of Fluids 18, 065106.

Wegner, B., Huai, Y., Sadiki, A., 2004. Comparative study of turbulent mixing in cross-flow configurations using LES. International Journal of Heat and Fluid Flow 25, 767–775.